DOI 10.1007/s11182-024-03232-y
Russian Physics Journal, Vol. 67, No. 8, August, 2024

FEATURES OF THE LATH MICROSTRUCTURE IN THE HEAT-AFFECTED ZONE OF THE 09G2S STEEL AFTER MANUAL ARC SURFACING

P. V. Kuznetsov UDC 539.24

Using scanning tunneling microscopy, it is shown that a lath structure is formed in the heat-affected zone of the low-carbon, low-alloy 09G2S steel after electric arc surfacing. Analysis of the results of scanning tunneling microscopy revealed a number of subtle morphological features of the lath structure, which makes it possible to explain the mechanism of its formation and identify it as lower bainite. The lower bainite structure in the heat-affected zone of the base metal of the 09G2S steel is favourable for increasing the impact strength of the coating – base metal composition, which was established earlier in our work.

Keywords: Low-carbon steel, intermediate transformation, ferrite, bainite, scanning tunnel microscopy.

INTRODUCTION

The study of bainitic transformation features in structural steels and the influence of bainitic structures on the mechanical properties of steel has been the main motivation for several generations of physical metallurgists [1]. Bainitic structures are formed in the intermediate temperature range between pearlite diffusion transformation and martensitic shear transformation and exhibit characteristic features of both, so the fundamental question of the mechanism of their formation remains under debate.

The formation of bainitic structures can occur as a result of special heat treatment or due to production conditions, for example, during welding or the use of electric arc surfacing [2, 3]. When a structure is formed under manufacturing conditions, several important transformation parameters, such as heating and cooling conditions, average austenite grain size, and temperature (and time) at which transformation begins vary and are difficult to control. Therefore, in contrast to structures obtained under isothermal conditions, structures formed under manufacturing conditions often do not have clearly defined morphological forms and unambiguous effect on the mechanical properties of steels [2–4].

The composition of the final microstructure and the morphology of the ferrite component significantly depend on the content of carbon and alloying elements [1, 3–5]. In low-alloy low-carbon steels, which are usually used for welded structures, the stability of austenite decreases due to the low carbon concentration, and the rate of bainite formation increases, while the upper limits of the bainite and martensitic transformation temperatures increase [1, 6]. The bainite transformation begins at high temperatures and is often kinetically not separated from the superimposed ferrite-pearlite transformation [6]. This leads to the formation of a mixture of various austenite transformation products, the identification of which requires the study of their subtle morphological features [1, 6].

In work [7], it was shown that the introduction of titanium carbonitride nanoparticles during manual electric arc surfacing on the 09G2S steel results in a refinement of the ferrite-pearlite structure compared to surfacing obtained using commercial electrodes. In addition, using scanning tunneling microscopy (STM), local areas of bainite and acicular ferrite were observed in the ferrite-pearlite structure of the surfacing. The grain refinement and the formation of

Institute of Strength Physics and Materials Science of the Siberian Branch of the Russian Academy of Sciences, Tomsk, Russia, e-mail: kpv@ispms.ru. Original article submitted July 30, 2024.

TABLE 1. Chemical Composition of the 09G2S Steel

	C	Mn	Si	Ni	Cr	N	Cu	As	P	S
Wt.%	0.1	1.3–1.7	0.5–0.8	up to 0.3	0.3	0.08	0.3	0.08	0.035	0.04

intermediate transformation structures in the surfacing led to an almost twofold increase in the fracture toughness of the *coating – base metal* composition compared to the composition obtained using commercial electrodes [7].

Using the STM, it was shown in [8] that in the gradient structure in the coating and overheating zone of the surfacing, finely dispersed structures of acicular ferrite, trostite, and globular bainite are observed, which contribute to an increase in the fracture toughness of the composition. However, the fine microstructure of the heat-affected zone of the base metal – the 09G2S steel – which also affects the mechanical properties of the composition has not yet been studied. The purpose of this work is to study, using the STM, the fine microstructure of the heat-affected zone of the base metal 09G2S steel, which was formed during coating by manual electric arc surfacing using electrodes modified with titanium carbonitride additives.

MATERIALS AND METHODS

In this work, the main material – the 09G2S steel coated using manual electric arc surfacing with 0.2 wt.% titanium carbonitride as an additive, was investigated. The materials, method of applying surfacing to the substrate, method of testing the *coating – base metal* composition for fracture toughness, test results, and studies of the structure of the surfacing were described in detail in our works [7, 8]. Therefore, we will limit ourselves to a brief description of the main metal, namely, the 09G2S steel. The chemical composition of the 09G2S steel is given in Table 1.

Plates $1 \times 10 \times 10$ mm^3 in size were cut in the heat-affected zone of the base metal parallel to the surfacing plane at a distance of 3 mm from the *coating – base metal* boundary from the samples for fracture testing. The structure was revealed by chemical etching with a 4% alcohol solution of nitric acid (nital). The fine steel structure was studied using a scanning tunneling microscope SMMT-2000 (Zelenograd) in constant current mode (I = 2 nA) at the voltage between the tip and the sample U = 100 mV.

RESULTS

Due to the ability to examine samples that require minimal preparation time, the STM allows one to quickly obtain a representative set of data on the microstructures under study. Using the STM, both typical ferrite-pearlite structures and structures, the morphological features of which require careful analysis, were observed in the heat-affected zone of the base metal. An example of this structure is shown in Fig. 1*a*. Figure 1*b* shows the cross sectional profiles along the directions marked by segments of straight lines *AB* and *BC* in Fig. 1*a*. The magnified image of the upper right central portion of Fig. 1*a* is shown in Fig. 1*c*, and Fig. 1*d* shows the cross sectional profiles along the directions shown by straight line segments *1–1′* and *2–2′* in Fig. 1*c*.

Figure 1*a* shows the boundary of two grains, marked by the dashed line *b–b′*, on which two packets of laths (subunits in the terminology of work [1]) nucleated and oriented in approximately the same directions within the upper and lower grains. In Fig. 1*b*, taking into account the difference between the scales of the units along the axes, it can be seen that the cross sectional profile of the top grain laths on the right side has a tent shape, which becomes more complex on the left side. On the left side of Fig. 1*b,* the cross sectional profile shows the integral shape of the relief formed by a superposition of sublaths with lengths of ~200–300 nm separated by steps with heights of ~10–30 nm from one another. The stepped cross sectional profile of the ferrite plates may indicate sympathetic nucleation and growth of the ferrite subunits by a *face-to-face* (FTF) mechanism [9].

Another feature of the upper grain laths in Fig. 1*a* is a series of boundaries across the direction of their growth, some of which are marked by light arrows *a–a′*. Fig. 1*a* and in more detail, Fig. 1*b* show that the nucleation of continuing laths occurs either in the spaces between previous laths or at their border. The boundaries across the

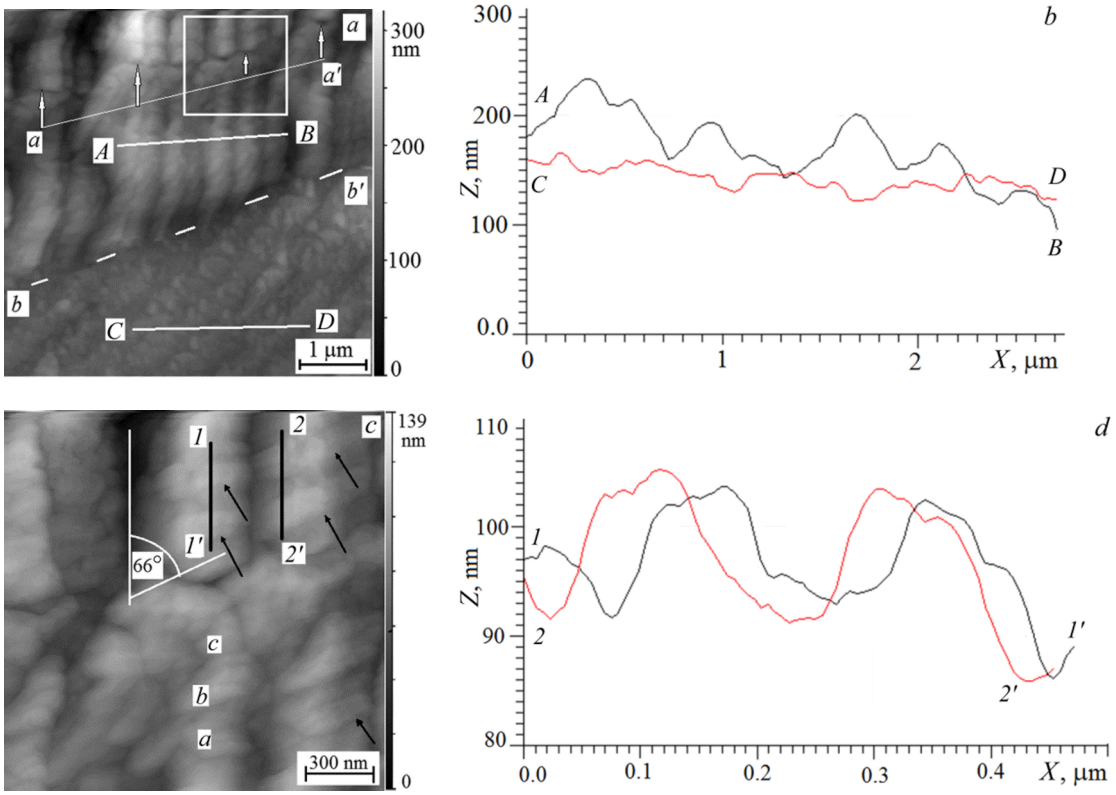

Fig. 1. STM images of the structures (*a* and *c*) with different magnifications, cross sectional profiles (*b*) along the directions indicated by straight line segments *A*–*B* and *C*–*D* in Fig. 1*a*, and cross sectional profile (*d*) along the direction shown by straight line segments *1*–*1′* and *2*–*2′* in Fig. 1*c*.

direction of lath growth are supposed to indicate the sympathetic nucleation and growth of laths of the *edge-to-edge* (ETE) type on previously formed laths at the austenite grain boundary [9].

Figure 1*a* shows that the top and bottom grain laths have a fine substructure, which is shown in more detail at higher magnification in Fig. 1*c* for the top grain. The lath substructure is formed from subsubunits with lengths of 250–300 nm designated, for example, by the letters *a*, *b*, and *c* in Fig. 1*c*. The boundaries of some subunits are approximately parallel, indicating that crystallographic orientations influence their formation.

In work [9], using the STM and transmission electron microscopy, it was shown that a bainite sheaf in a Fe–C–Cr–Si alloy consists of subunits – laths, which consist of subsubunits – and that the subsubunits also consist of subsubsubunits. A complex substructure of bainite was observed both when studying the relief formed during the austenite transformation in steel due to special heat treatment and after etching the structure with nital. The results were explained within the framework of the model of sympathetic nucleation and growth of bainite subunits [9].

At a higher STM resolution, a series of light stripes ~100 nm wide are revealed on the surface of the laths, marked by dark arrows in Fig. 1*c*. The long axes of the strips are oriented at an angle of approximately 66° relative to the direction of lath growth, as shown in Fig. 1*c*. The cross sections in Fig. 1*c* in the directions indicated by straight line segments *1*–*1′* and *2*–*2′* in Fig. 1*c* show that the stripes rise to a height of ~10–20 nm above the level of the ferrite laths.

This indicates that the rate of chemical etching with nital was lower than the rate of etching of the ferrite laths. According to work [10], nital preferentially etches ferrite, leaving austenite and cementite intact. In addition, the ferrite-based phases such as bainitic and pearlitic ferrites dissolve and have a typical morphology that allows them to be recognized [10]. This suggests that the stripes are either cementite or austenite. This issue will be discussed in more detail below.

DISCUSSION

The lath structure similar to that observed in the upper and lower grains in Fig. 1*a* is typical for Windmanstätten ferrite, upper bainite, and lower bainite in low-carbon steels [1]. These structures can nucleate at the boundaries of the initial austenite grains and differ in their growth mechanism [1]. Windmanstätten ferrite nucleates and grows at high temperatures and, due to the rapid diffusion of carbon, appears homogeneous, without an internal structure [11, 12]. Bainitic ferrite, unlike Windmanstätten ferrite, has the complex hierarchical structure consisting of subunits, subsubunits, and subsubsubunits, which are revealed by nital and can be observed via the STM [9]. Therefore, the substructure in the laths of the upper and lower grains in Fig. 1 allows us to conclude that the laths are bainite ferrite rather than Windmanstätten ferrite.

There are two alternative viewpoints regarding the mechanism of formation of the ferrite component of bainite and, in particular, their subunits. One school of thought believes that the ferrite component of bainite develops over the entire range of bainitic temperatures by the diffusion ledge mechanism, similar to the assumptions made to explain the formation of Widmannstetten preeutectoid ferrite [1]. The carbon content of this ferrite is considered to be between the $\alpha/\alpha + \theta$ phase boundaries and the extrapolated $\alpha/\alpha + \gamma$ phase boundaries, and bainitic carbides are believed to be formed primarily at the austenite-ferrite interface [1, 13].

The opposing school of thought suggests that bainite is formed by a shear mechanism and is a collection of discrete subunits of bainitic ferrite formed directly by shear and retained austenite or carbides (cementite) that is formed by secondary reactions [1,13]. Bainite grows without diffusion in the form of tiny platelets known as *subunits*, which are the phase change units of bainitic ferrite and are characterized by a regular shape, a defined habit plane, and crystallographic relationships with the parent phase. They grow to a limited size, which is determined by the plastic accommodation of shape deformation accompanying the transformation [1].

In Fig. 1*a* and *c* it can be seen that the shape and size of the subunits of the laths of the upper grain vary, which does not allow us to draw conclusions about the shear mechanism of their formation. The shape and size of the substructure of the lower-grain laths are even more chaotic; therefore, their formation due to the shear mechanism is even less likely than that of the upper-grain laths.

Thus, analysis of the STM images of the structures in Fig. 1 shows that the morphology of the ferrite laths of the upper grain reveals characteristic signs of simultaneous sympathetic nucleation and growth of the FTF and ETE types in two main directions [9]. Sympathetic nucleation is defined in [9, 14] as the nucleation of a precipitate crystal at the interface of a crystal of the same phase when these crystals differ in compositions from their matrix phase throughout the entire transformation process. The nucleus of the new ferrite phase is supposed to be formed from the very beginning and has a common face with the austenitic matrix, i.e., the nucleus is in contact with the initial phase, and the interphase boundary is coherent or semicoherent, which ensures its low energy. Due to the low interfacial energy, none of the wide faces of lamellar deposits can migrate in the perpendicular direction [9]. However, some structural ledge risers at the lateral interface become incoherent, for example, due to thermal activation, and can migrate laterally due to volume diffusion, allowing the growth of the bainite plate. The growth rate of bainite platelets is controlled by the composition gradient and volume diffusion of dissolved carbon atoms in the austenite near the interface. During the lateral migration of a growing step on a wide face of the parent phase, according to works [9, 14], the bainite plate thickens, and an increasing amount of carbon is pushed out from the growing ferrite phase into austenite at the front of the migrating step. This leads to a change in the concentration profile of dissolved carbon atoms at the ferrite/austenite boundary near the step towards a decrease in the concentration gradient. As a result, the driving force for plate growth and the step migration speed decrease over time. At the same time, another ferrite nucleus can nucleate on the wide face after the incubation period, and the process repeats leading to the formation of a new bainite plate [9, 14]. Thus, a package of ferrite plates is formed due to lateral growth, which in cross section has the shape of elongated flat sections separated by steps, similar to that seen in Fig. 1*b*. Similar processes of stopping and continuing lath growth in the longitudinal direction lead to the formation of boundaries in the transverse direction (Fig. 1*a*). The sympathetic nucleation of continuing laths of the ETE type occurs on the partially coherent faces of the interphase boundaries and in the areas between the growth projections of previous laths (Fig. 1*a* and *c*) [15].

As reported in work [9], if the FTF- and ETE-type sympathetic nucleation reactions occur simultaneously, a lower bainitic structure will be formed. A feature of lower bainite is the precipitation of carbides. Carbides nucleate

between subunits of lower bainite at an angle of 60–70° to the longitudinal direction of growth of ferrite plates at the austenite/ferrite interface and grow towards austenite, which is explained by the mechanism of step-like growth controlled by diffusion [9].

The results obtained using the STM are in good agreement with the ideas about the carbide precipitation in lower bainite [9]. Assuming that the strips in Fig. 1*c*, rising above the level of the surrounding ferrite to a height of ~10–20 nm due to the lower etching rate with nital that are oriented with their long axis at an angle of 66° relative to the longitudinal direction of growth of the laths are particles of carbides, we can conclude that the lath structure in the upper grain in Fig. 1*a* and *c* is a sheaf of lower bainite.

The differences in the lath morphology of the upper and lower grains may indicate that they are formed at different stages of transformation, which can be associated with their different carbon contents. At lower carbon content, the austenite decomposition begins earlier and at a higher temperature when the austenite is mechanically weak due to its lower yield strength. The shape change accompanying the austenite/ferritic transformation is accommodated at least partially by plastic relaxation of austenite and the formation of a high dislocation density, which ultimately blocks the transformation boundary due to loss of coherence [16]. Then the resulting dislocation debris introduced into the austenite can be inherited by any ferrite subsequently formed and can appear as subsubunits of the laths. Another possible consequence of the formation of a high dislocation density is the segregation of carbon on dislocations, which is redistributed from the supersaturated bainitic ferrite to the austenite, leading to the formation of the carbide-free bainite [16].

CONCLUSIONS

In this work, the lath structure was observed via the STM in the heat-affected zone of the base metal 09G2S steel formed during coating by manual electric arc surfacing using electrodes modified with titanium carbonitride additives. The analysis of the STM images of the lath structure revealed a set of subtle morphological features that have made it possible to identify it as the lower bainite and explain the mechanism of its formation. The formation of the lower bainite occurs under conditions of continuous cooling according to the mechanism of sympathetic nucleation and growth of the PTF and ETE types in two main directions and provides a multi-level structure of laths, which is a favourable factor in ensuring high impact strength of the *coating – base metal* composition.

COMPLIANCE WITH ETHICAL STANDARDS

Conflicts of interest

The author has no competing interests to declare that are relevant to the content of this article.

Funding

This work was carried out at the Institute of Strength Physics and Materials Science of the Siberian Branch of the Russian Academy of Sciences within the framework of Government Contract FWRW-2021-0009.

Financial interests

The author has no relevant financial or non-financial interests to disclose.

Institutional review board statement

Applicable.

REFERENCES

1. H. K. D. H. Bhadeshia, Bainite in Steels. Theory and Practice, CRC Press, London (2015); https://doi.org/10.1201/9781315096674.
2. D. V. Edmonds and R.C. Cochrane, Metall. Trans. A, **21**, 1527–1540 (1990); https://doi.org/10.1007/BF02672567.
3. O. Grong and D. K. Matlock, International Metals Reviews, **31** No. 1, 27–38 (1986); https://doi.org/10.1179/imtr.1986.31.1.27.
4. B. L. Bramfitt and J. G. Speer, Metall. Trans. A, **21**, No. 3, 817–829 (1990); https://doi.org/10.1007/BF02656565.
5. A. Yu. Kaletin, Yu. V. Kaletina, and M. A. Ryzhkov, Lett. Mater., **10**, No. 3, 249–253 (2020); https://doi.org/10.22226/2410-3535-2020-3-249-253.
6. V. M. Schastlivtsev, T. I. Tabatchikova, I. L. Yakovleva, *et al*., Iss. Mater. Sci., No. 3, 26–38 (2009).
7. P. V. Kuznetsov, N. K. Galchenko, and Yu. I. Pochivalov, Crystals, **13**, 146 (2023); https://doi.org/10.3390/cryst.13010146.
8. P. V. Kuznetsov, N. K. Galchenko, I. V. Belyaeva, *et al*., Russ. Phys. J., **64**, No. 4, 605–611 (2021); https://doi.org/10.1007/s11182-021-02383-6.
9. H. S. Fang, J. J. Wang, Z. G. Yang, *et al*., Metall. Mater. Trans. A, 27A, 1535–1545 (1996); https://doi.org/10.1007/BF02649813.
10. E. Girault, P. Jacques, Ph. Harlet, *et al*., Mater. Charact., **40**, 111–118 (1998); https://doi.org/10.1016/S1044-5803(97)00154-X.
11. G. Krauss and S. W. Thomson, ISIJ Int., **35**, No 8, 937–945 (1995); https://doi.org/10.2355/isijinternational.35.937.
12. H. G. Yang, J. J. Wang, C. M. Li, *et al*., J. Mat. Sci. Lett., **17**, 331–333 (1998); https://doi.org/10.1023/A:1006550126306.
13. H. K. D. H. Bhadeshia and D. V. Edmonds, Metall. Trans. A, **10**, 895–907 (1979); https://doi.org/10.1007/BF02658309.
14. R. F. Hehemann, K. R. Kinsman, and H. I. Aaronson, Metall. Trans., **3**, 1077–1094 (1972); https://doi.org/10.1007/BF02642439.
15. E. Sarath Kumar Menon and H. I. Aaronson, Acta Metall., **35**, No. 3, 549–563 (1987); doi:10.1016/0001-6160(87)90179-9.
16. F. G. Caballero, Carbide-Free Bainite in Steels, in: Phase Transformations in Steels. Fundamentals and Diffusion-Controlled Transformations, Vol. 1, Ch. 12, Woodhead Publishing Series in Metals and Surface Engineering (2012), pp. 436-467; https://doi.org/10.1533/9780857096104.3.43.